Multi-Cycle Control Rod Design Optimization for a Soluble Boron Free i-SMR Using Multi-Objective Simulated Annealing

Woo Jin Lee [a] , Ser Gi Hong [a*], Jin Sun Kim[b*]
[a] Departments of Nuclear Engineering, Hanyang University, 222, Wangsimni-ro, Seongdong-gu, Seoul, 04761, Republic of Korea
[b] KEPCO Nuclear Fuel Co. Ltd., 242, Deadeok-daero 989beon-gil, Yuseong-gu Daejeon, 34507, Republic of Korea

[a*]*Corresponding author: hongsergi@hanyang.ac.kr*

Keywords : Soluble-Boron Free i-SMR, Control rod design optimization, Simulated annealing

1. Introduction

In a soluble-boron-free (SBF) core, reactivity control is achieved entirely by control rods (CR). Therefore, optimization of CR design is important to ensure safe operation of an SBF core. Key CR design variables include the CR layout, absorber material, insertion order, and overlap length. These variables must be combined so that ASI, F_q, F_r, F_{xy} satisfy their respective design limits throughout the cycle. At the same time, sufficient cycle length must be considered from an economic standpoint.

Simulated annealing (SA) is known to be effective for global optimization because it can escape local optima by probabilistically accepting worse solutions. In nuclear core design, SA has been applied mainly to fuel loading pattern optimization, while its application to CR design optimization for SBF cores has been less explored. Therefore, this study employs SA to perform multi-cycle CR design optimization for an SBF core. The CR design optimization uses four design variables: CR bank layout, CR absorber material, CR insertion order, and CR overlap length.

The SA acceptance probability is calculated using the discontinuous penalty function (DPF) proposed in [1]. For each cycle, the DPF imposes constraints on the ASI swing, peak F_q, peak F_r, peak F_{xy}, and minimum cycle length, and also includes total cycle-length sum across all cycles. Each term is zero when its limit is satisfied and increases quadratically with the magnitude of any violation. To drive cycle-length extension, the adaptive-constraint DPF [2] is also applied to progressively raises the target of total cycle-length sum whenever a newly found fully feasible solution exceeds the current bound. A positional penalty is additionally included to reduce the likelihood of assigning CR banks to designated core locations. The SA acceptance probability is then calculated by the total objective J(X), defined as the sum of the cycle-wise DPFs (cycles 1 to N) plus the positional penalty.

The target system is a SBF i-SMR. Two core designs are considered: (1) a core developed by KNF [3] and (2) the other core previously developed by our group [4]. For each core design with the corresponding loading pattern, the SA algorithm developed in this study is applied to obtain an optimized CR design. Core calculations are performed using the KAERI DeCART2D/MASTER code system [5,6].

2. Design and Methodologies

2.1 Target core design

Table I summarizes the key design parameters used for SA-based CR optimization. The target system is a 520 MW_{th} i-SMR core with 69 fuel assemblies (17×17) and a 240 cm active fuel height. Two core designs were analyzed: Design 1, a KNF core employing enriched gadolinium burnable absorbers (UO_2–Gd_2O_3) [3], and Design 2, a core previously developed by our group using GdN-CBA [4]. Although the two designs have the same reactor configuration, their cycle-wise excess reactivity profiles differ, leading to different CR movement histories for reactivity control and, consequently, different trends in core safety parameters and cycle length. Moreover, the two designs use different numbers of CR fingers, which further affect the CR worth and operational characteristics. Therefore, SA is employed to examine whether it can robustly optimize the CR design for both cores while satisfying safety constraints and maximizing cycle length.

Table I: Key design parameters of the two SBF i-SMR cores considered in this study.

	Design 1 [3]	**Design 2 [4]**
Core thermal power	520 MW_{th}	
Number of FA	69	
FA array	17x17	
Active fuel height	240 cm	
Fuel management	2 batches	
Burnable absorber	UO_2-Gd_2O_3	GdN-CBA
Number of fingers in CR assembly	28	24

2.2 Multi-Cycle CR design Optimization Methodology

Table II summarizes the optimization variables and their search domains defined in this study for SA-based CR design optimization. In this work, SA is applied to optimize the CR design by identifying an optimal design

variable **X** that simultaneously satisfies core safety constraints and cycle length. The design variable **X** consists of four variables: (1) CR bank layout, (2) CR overlap length, (3) CR insertion order, and (4) CR absorber material. The search domain and the number of cases are defined for each core design, as described below:

1) **CR bank layout:** under 1/8 symmetry, 13 CR locations are available. After excluding 2, 3 locations for TM-ICI, 10 (Design 1) and 11 (Design 2) free positions remain. The R banks (R1 to R4) are distinguished, while the S banks are treated as indistinguishable. Accordingly, the number of layout cases is $^{10}P_4$=5040 for design 1 and $^{11}P_4$=7920 for design 2.
2) **CR overlap length:** The overlap length range was selected to correspond to approximately 30–60% of the 240 cm CR absorber length. Accordingly, the overlap length varies from 75 to 145 cm in 5 cm increments, yielding 15 cases
3) **CR insertion order:** The insertion sequence is determined by selecting three out of four R banks and ordering them, resulting in $\binom{4}{3}$ x 3! = 24 cases.
4) **CR absorber material:** Two CR absorber types (CR1 and CR2) are considered, as shown in Table II. Among the three inserted R banks, 0–2 banks may adopt CR2 in design 1, whereas 0–3 banks may adopt CR2 in design 2. The remaining banks use CR1. This yields $\sum_{k=0}^{2}\binom{3}{k} = 7$ cases for design 1 and $\sum_{k=0}^{3}\binom{3}{k} = 8$ for design 2. For both designs, the shutdown bank (S bank) absorber material is fixed to B_4C enriched to 95 a/o ^{10}B.

   (Note: CR2 is adopted as a gray rod [7] with reduced neutron absorption to mitigate power-distribution distortions during CR movement. Therefore, it is included in the SA search space to provide additional flexibility for identifying improved designs. As shown in Fig. 1, the gray rod configuration is modeled by replacing a portion of absorber fingers with non-absorber fingers.)

The total number of cases is 12,700,800 for design 1 and 22,809,600 for design 2. Such large search spaces make it impractical to evaluate every possible case. Thus, SA is adopted to efficiently search for near-optimal solutions.

Table II: Optimization variables and search domains defined in this study for SA-based CR design optimization.

CR variable X		Design 1	Design 2
Layout		R1~R4, S1~S6 (10 free positions)	R1~R4, S1~S7 (11 free positions)
Overlap length		75~145 cm (5cm step)	
Insertion order		Choose 3 of 4 R banks and determine the insertion order	
Absorber material *	CR 1	28 AIC finger	24 AIC
	CR 2	16 AIC / 12 Steel finger	4 AIC / 20 Inconel finger

** Note: Within the inserted R banks, 0 to 2 banks are assigned the CR2 type (remaining R banks use CR1 type)*

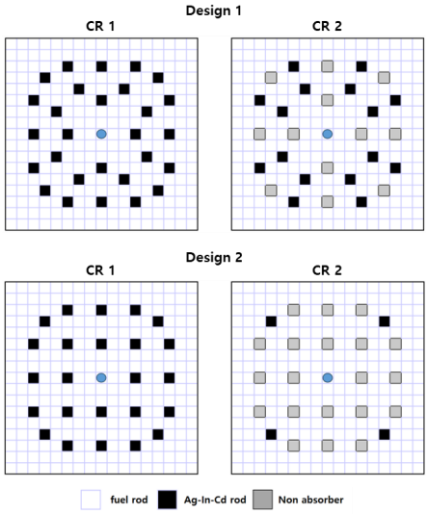

Fig. 1. CR1 and CR2 configurations for SA in both core designs.

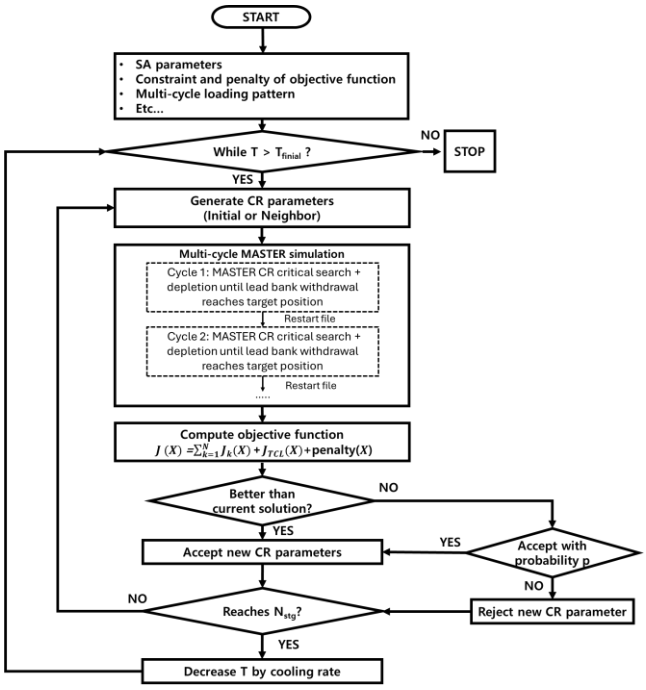

Fig. 2. Overall procedure of the SA based multi-cycle CR design optimization.

Fig. 2 shows the overall procedure of the SA-based multi-cycle CR design optimization. Before the SA loop, the SA parameters (initial temperature, cooling rate, and terminal temperature, iterations per temperature level, stagnation criterion) are specified. In this study, they were set to 50, 0.9, and 0.001, 20, and 1500, respectively.

The target constraints and penalty-function settings used in the objective function are also provided based on assumed design targets. Multi-cycle loading patterns are required as inputs, and the optimization was performed for four cycles (Cycles 1~4). When the SA loop starts, an initial solution **X** is generated, either randomly or by user specification. In this study, the initial solution was set to reference design. Each solution **X** is then written to the MASTER input via a script, and the core calculations

are executed sequentially over multi-cycles by linking restart files. For each cycle, the cycle length is defined as the EFPD at which the lead bank reaches a prescribed critical position. This endpoint is determined automatically using an external Python module that monitors the MASTER outputs and explicitly determines the cycle length.

The quality of a solution **X** is measured using the total objective function, which is evaluated after completing the sequential multi-cycle MASTER calculations.

1) Total objective

$$J(X) = \sum_{k=1}^{4} J_k(X) + J_{TCL}(X) + \text{Penalty}(X) \quad (1)$$

2) $J_k(X)$

$$J_k(X) = \sum_{i=1}^{5} f(\delta_{i,k}, \sigma_{i,k}), \quad (2)$$

$$f\left(\delta_{i,k}, \sigma_{i,k}\right) = \begin{cases} 1 + \dfrac{\delta_{i,k}^2}{\sigma_{i,k}^2}, & \delta > 0 \\ 0, & \delta \le 0 \end{cases}$$

$$Where\ \delta_{1,k} = \Delta ASI_k - \Delta ASI_k^{lim} \quad (3)$$

$$\delta_{2,k} = F_{q,k}^{max} - F_{q,k}^{lim} \quad (4)$$

$$\delta_{3,k} = F_{r,k}^{max} - F_{r,k}^{lim} \quad (5)$$

$$\delta_{4,k} = F_{xy,k}^{max} - F_{xy,k}^{lim} \quad (6)$$

$$\delta_{5,k} = L_k^{target} - L_k \quad (7)$$

3) $J_{TCL}(X)$

$$J_{TCL}(X) = \begin{cases} 1 + \dfrac{\delta_{L_{sum}}^2}{\sigma_{L_{sum}}^2}, & \delta > 0 \\ 0, & \delta \le 0 \end{cases} \quad (8)$$

$$Where\ \delta_{L_{sum}} = L_{sum}^{target} - \sum_{k=1}^{N} L_k \quad (9)$$

Equations (1) ~ (9) define the total objective function to evaluate solution **X** in the SA algorithm. As shown in Eq. (1), $J(\mathrm{X})$ consists of the sum of cycle-wise penalty functions $J_k(\mathrm{X})$ over four cycles, the total cycle-length penalty $J_{\mathrm{TCL}}(\mathrm{X})$ and an additional term $\mathrm{Penalty(X)}$. For each cycle k, $J_k(\mathrm{X})$ (Eq. (2)) is calculated from five constraint penalties using the discontinuous penalty function [1], which is zero when a constraint is satisfied ($\delta \le 0$) and increases quadratically when violated ($\delta > 0$), with σ as a normalization constant.

The violation terms $\delta_{i,k}$ (Eqs. (3) ~ (7)) quantify exceedances of the ASI swing limit, the cycle-wise peak limits of F_q, F_r, and F_{xy}, and the shortfall from the target cycle length L_k^{target}. The total cycle-length penalty $J_{\mathrm{TCL}}(\mathrm{X})$ (Eqs. (8), (9)) penalizes any shortfall of the cumulative cycle length from $L_{\mathrm{sum}}^{\mathrm{target}}$. Under the adaptive-constraint scheme [2], $L_{\mathrm{sum}}^{\mathrm{target}}$ is updated to the achieved $\sum_{k=1}^{N} L_k$ whenever a fully feasible solution is found (i.e., $\sum_k J_k(\mathrm{X}) = 0$ and $\mathrm{Penalty(X)} = 0$), which helps find designs with longer total cycle length while still meeting the constraints. The additional penalty term $\mathrm{Penalty(X)}$ assigns a penalty when any R bank is placed at a designated core location, and an extra penalty when the R bank located at that position is selected as the first bank in the insertion (lead-bank) sequence.

Once the objective $J(\mathbf{X})$ is evaluated, the solution is accepted or rejected according to the SA acceptance rule, which probabilistically allows worse solutions based on the current temperature.

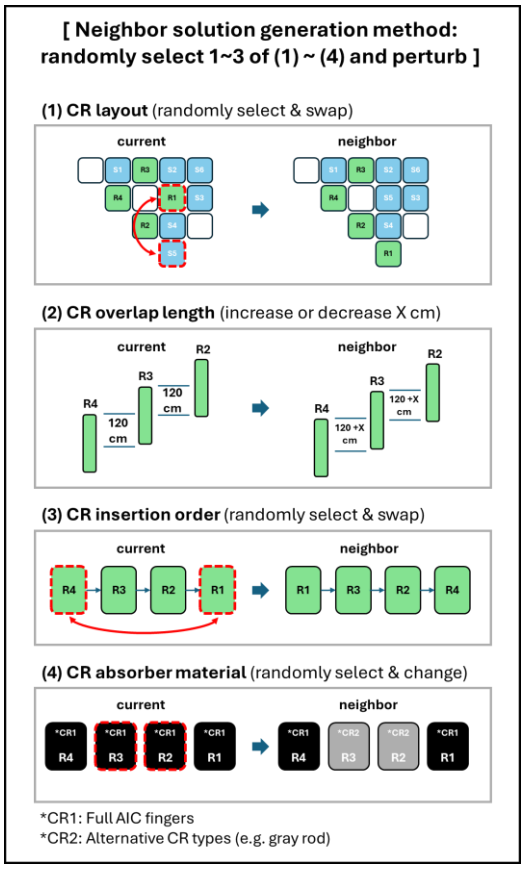

Fig. 3 Neighbor solution generation method for SA in CR design optimization.

After the initial solution is evaluated, a neighbor solution is generated according to the rule illustrated in Fig. 3 (layout swap, overlap-length perturbation, insertion-order swap, and absorber-type change). The same evaluation and SA acceptance procedure is then repeated iteratively until the termination temperature is reached.

This SA-based optimization procedure was independently applied to both core designs (design 1 and design 2). For each design, the optimized CR solution obtained by SA was then compared with the corresponding reference design to evaluate the improvement in core safety parameters and cycle-length performance.

3. Numerical Results and Analysis

Figures 4 and 5 show the convergence histories of the SA optimization for the multi-cycle CR design problem. In both cases, the SA search was carried out for more than 1800 iterations. During the high temperature region, worse solutions were accepted with relatively high probability, resulting in large fluctuations in the cycle-wise safety parameters and EFPD values. As the temperature decreased, the acceptance probability for worse solutions was reduced, and the search gradually concentrated on improved feasible regions. After approximately 750 iterations for design 1 and 1000 iterations for design 2, the major parameters (ASI variation, peak F_q, peak F_r, peak F_{xy}, cycle-wise EFPD, and total EFPD) showed clear convergence trends, with only minor changes thereafter.

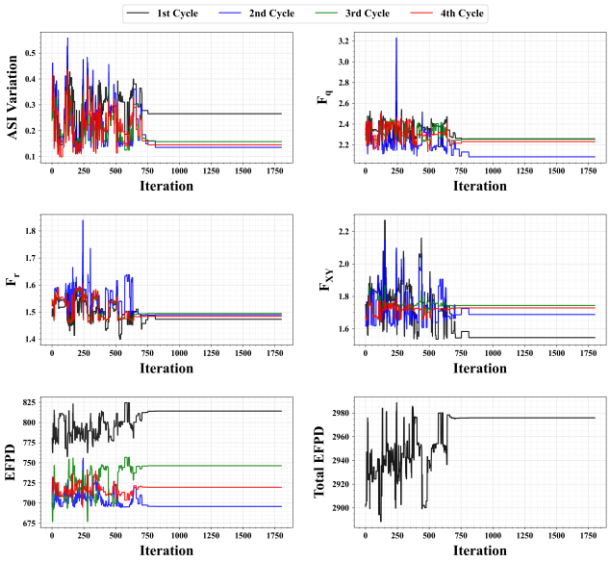

Fig. 4 SA convergence behavior of multi-cycle core safety parameters and cycle-length (Design 1).

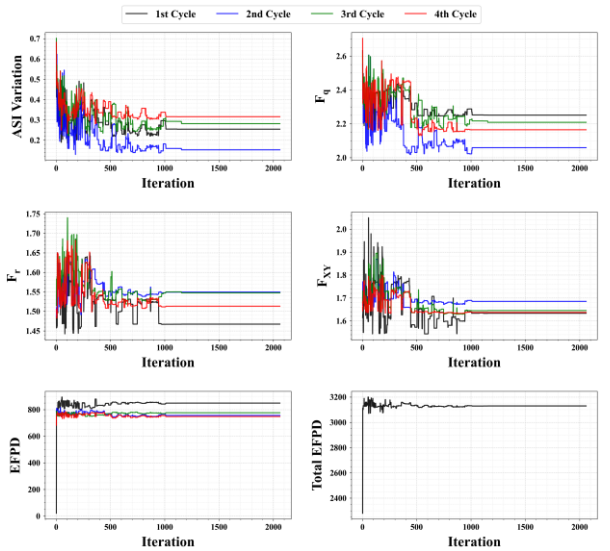

Fig. 5 SA convergence behavior of multi-cycle core safety parameters and cycle-length (Design 2).

Table III summarizes the SA optimization performance for design 1 and 2. $N_{feasible}$ denotes the number of solutions satisfying the target constraints, for which the objective-function components (all cycle-wise constraints and the total cycle-length target are satisfied). Among the SA iterations, 19 feasible solutions were identified for design 1, while 7 feasible solutions were identified for design 2. N_{pass} denotes the number of feasible solutions that satisfy the subcriticality criteria at cold zero power under all-rods-in and N-1 stuck-rod conditions. Specifically, the accepted solutions satisfy the subcriticality requirements of $k_{eff} < 0.95$ and $k_{eff} < 0.99$ (N-1 stuck rod). Under these criteria, 10 solutions passed for design 1 and 2 solutions passed for design 2.

The computation time of design 2 was more than twice that of design 1, mainly because a different EOC lead-bank position criterion was used for cycle-length determination and more SA iterations were performed.

Fig. 6 and Table IV show the SA-optimized solutions for designs 1 and 2, chosen from the N_{pass} solution set (obtained at the iterations 1652, 1722 repectively). The selected layouts are generally similar to the reference layouts, but with several bank positions rearranged. The CR insertion order was identified as R4→R3→R2→R1 for both designs. The optimized CR overlap length was reduced from the reference value of 120 cm to 110 cm (design 1) and 75 cm (design 2). For the absorber-material configuration, CR2 was assigned to two R-banks in design 1 and three R-banks in design 2.

Table III. Summary of SA optimization performance for Designs 1 and 2.

Parameters	**Design 1**	**Design 2**
Calculation time	25 hr 54 m	59 hr 46 m
Number of SA iteration	1800	2060
$N_{feasible}$	19	7
N_{pass}	10	2

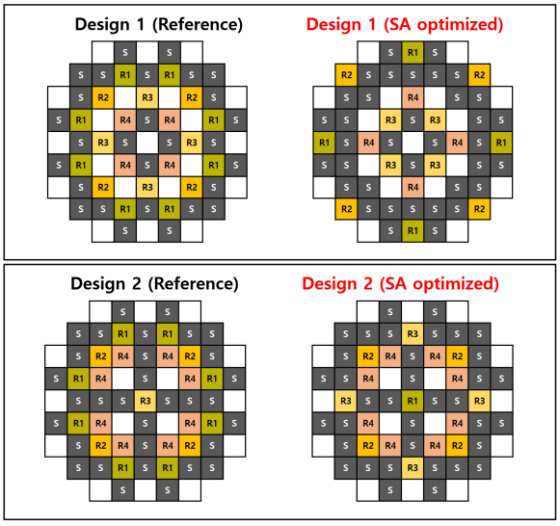

Fig. 6 Selected solution (layouts) for design 1 and 2 from the N_{pass} solutions.

Table IV: Selected solution (overlap length, insertion order, absorber material) for design 1 and 2 from N_{pass} solutions.

		Design 1	Design 2
CR overlap length		110 cm	75 cm
CR insertion order		R4→ R3→ R2→ R1	
CR absorber material	R4	CR2	CR2
	R3	CR2	CR2
	R2	CR1	CR2
	R1	CR1	CR1

Figures 7 and 8 and Table V compare the cycle-wise performance of the reference and SA-optimized CR designs for Designs 1 and 2. Overall, the SA-optimized designs show improved or comparable core safety performance across most cycles, while also maintaining or improving cycle-length performance. In particular, the SA solutions generally reduce the ASI variation and the peak F_q and F_r values in many cycles, indicating improved control of power-shape behavior and peaking factors. This improvement is attributed to the inclusion of the gray-rod option (CR2) in the SA optimization domain, whose lower rod worth helps mitigate power-distribution distortions during CR movement. The F_{xy} values remain comparable, with some cycles showing improvement and others showing slightly higher values.

In terms of cycle length, the SA-optimized designs show an overall favorable trend, with noticeable gains in several cycles while maintaining similar performance in others. Because the cycle length was compared using the same EOC lead bank position, the observed extension is likely attributable to improved power-shape control (i.e., a flatter power distribution), which allows longer depletion before reaching the same lead-bank position.

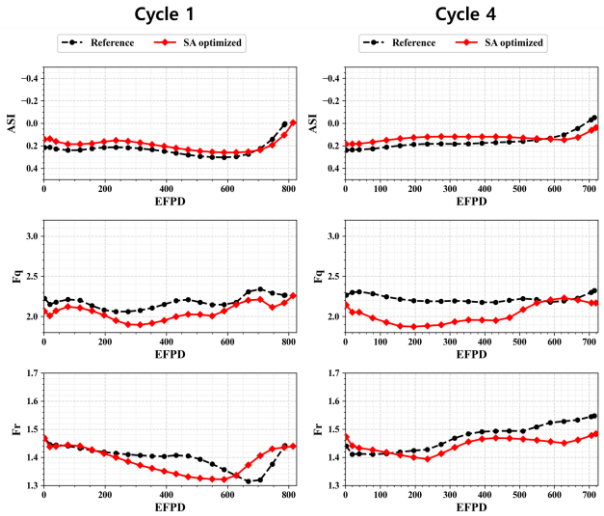

Fig. 7 Design 1 results: ASI, F_q, and F_r profiles for the reference and SA-optimized CR designs.

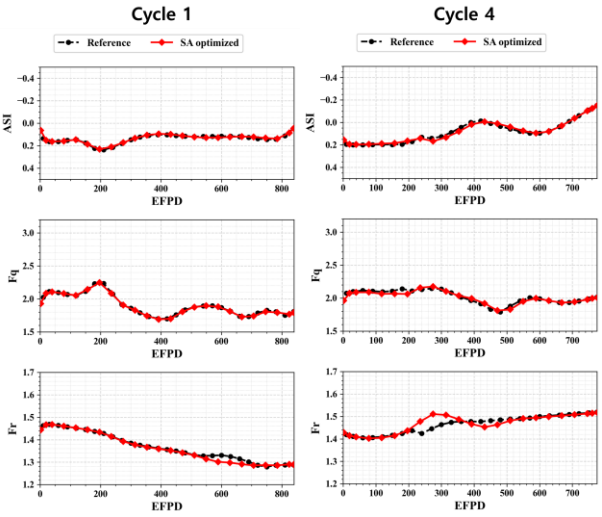

Fig. 8 Design 2 results: ASI, F_q, and F_r profiles for the reference and SA-optimized CR designs.

Table V: Comparison of core safety parameters and cycle length between the reference and SA-optimized designs for designs 1 and 2.

		Design 1 (SA / Reference)	Design 2 (SA / Reference)
ASI_{var}	1st	**0.265** / 0.276	**0.187** / 0.223
	2nd	**0.135** / 0.243	**0.149** / 0.179
	3rd	**0.157** / 0.240	**0.244** / 0.279
	4th	**0.145** / 0.270	**0.345** / 0.351
F_q	1st	**2.257** / 2.341	**2.247** / 2.259
	2nd	**2.084** / 2.288	**2.085** / 2.080
	3rd	**2.253** / 2.248	**2.163** / 2.165
	4th	**2.230** / 2.300	**2.176** / 2.148
F_r	1st	**1.472** / 1.481	**1.467** / 1.529
	2nd	**1.489** / 1.522	**1.550** / 1.548
	3rd	**1.494** / 1.546	**1.544** / 1.535
	4th	**1.483** / 1.543	**1.517** / 1.519
F_{xy}	1st	**1.545** / 1.733	**1.644** / 1.567
	2nd	**1.687** / 1.622	**1.682** / 1.682
	3rd	**1.743** / 1.675	**1.649** / 1.647
	4th	**1.728** / 1.666	**1.639** / 1.641
EFPD	1st	**814.0** / 781.2	**839.4** / 839.0
	2nd	**695.8** / 696.3	**760.6** / 760.1
	3rd	**746.3** / 713.1	**771.6** / 769.7
	4th	**719.6** / 711.1	**776.1** / 774.4

This study shows that the proposed SA-based multi-cycle CR optimization can effectively improve safety-related core parameters and cycle-length performance.

As future work, further development of the SA algorithm will be carried out, including the application of adaptive SA parameter settings, modification of random-solution generation rules, and implementation of parallel computing strategies to improve computational efficiency. In addition, the optimization framework will be extended to flexible operation scenarios.

4. Conclusions

In this study, a SA-based multi-cycle CR design optimization was developed and applied to a soluble-

SBF i-SMR cores. The proposed method optimized four CR design variables (CR bank layout, overlap length, insertion order, and absorber material) under multi-cycle conditions by using a DPF-based objective function with adaptive total-cycle-length constraints.

The SA optimizations was implemented with the DeCART2D/MASTER code system and sequential multi-cycle depletion calculations linked through restart files. The proposed SA optimizations was applied to two different SBF i-SMR core designs with different burnable absorber concepts and reactivity profiles. The results showed that the proposed SA optimizations can effectively identify CR designs that satisfy the prescribed safety-related constraints while improving, or maintaining, cycle-length performance.

As future work, further development of the SA algorithm will be carried out, including the application of adaptive SA parameter settings, improvement of random-solution generation rules, and implementation of parallel computing strategies to improve computational efficiency. In addition, the optimization will be extended to flexible operation scenarios.

Acknowledgment

This work was supported by the Innovative Small Modular Reactor Development Agency grant funded by the Korea Government (MCEE) (No. RS-2024-00407975) and by the Nuclear Safety Research Program through the Regulatory Research Management Agency for SMRs (RMAS) and the Nuclear Safety and Security Commission (NSSC) of the Republic of Korea (No. RS-2024-00509678)

References

[1] Park, T. K., Joo, H. G., Kim, C. H., & Lee, H. C. (2009). Multiobjective loading pattern optimization by simulated annealing employing discontinuous penalty function and screening technique. *Nuclear Science and Engineering*, *162*(2), 134-147.

[2] Park, T. K., Joo, H. G., & Kim, C. H. (2014). Multicycle fuel loading pattern optimization by multiobjective simulated annealing employing adaptively constrained discontinuous penalty function. Nuclear Science and Engineering, 176(2), 226-239.

[3] Kim, J. S., Bae, G., & Yoon, J. (2024). Reactor core design with enriched gadolinia burnable absorbers for soluble Boron-Free operation in the innovative SMR. Nuclear Engineering and Design, 428, 113557.

[4] Lee, W. J., Cho, S. H., Choi, S. H., & Hong, S. G. (2025). Application and analysis of Cr-coated GdN-CBA to i-SMR core with two control rod patterns for load-following operations. Nuclear Engineering and Technology, 104029.

[5] J.Y. Cho, et al., DeCART2D v1.1 user's manual, KAERI/UM-40/2016 (2016).

[6] J.Y. Cho, et al., MASTER v4.0 user's manual, KAERI/UM-41/2016 (2016)

[7] M. Onoue, T. Kawanishi, W.R. Carlson, T. Morita, Application of MSHIM Core Control Strategy for Westinghouse AP1000 Nuclear Power Plant, 2011.